Comparative Study of Silicon nanowires Grown from Ga, In, Sn and Bi for Energy Harvesting

Krishna Nama Manjunatha, Iulia Salaoru, W.I Milne and Shashi Paul

***Abstract*—A high density of silicon nanowires for solar cell applications was fabricated on a single crystalline silicon wafer, using low eutectic temperature metal catalysts namely; gallium, indium, tin and bismuth. The use of silicon nanowires is exploited for light trapping with an aim to enhance the efficiency of solar cells. Additionally, we have optimised the deposition parameters so that there is merely deposition of amorphous silicon along with the growth of silicon nanowires. Thus, it may improve the stability of silicon based solar cells. The different catalysts used are extensively discussed with experimental results indicating stable growth and highly efficient silicon nanowires for photovoltaic applications. To test the stability, we measured the open circuit voltage for four hours and the change in voltage was ±0.05V. The fabrication of all-crystalline silicon solar cells was demonstrated using the conventional mature industrial manufacturing process that is presently used for the amorphous silicon solar cells. To summarise, this research compares various post-transition metals as a catalyst for the growth of nanowires discussing their properties, and such silicon nanowires can be utilised in several other applications not only limited to photovoltaic research.**

***Index Terms* — Catalyst, Eutectic Temperature, Nanowires, PECVD, Silicon Nanowires, Solar cell, wafer-wire junction.**

I. Introduction

Demand for renewable energy sources such as biomass, hydroelectricity, wind and solar energy is being increasingly debated. They are abundantly available, cheap, non-toxic and do not pollute the environment. Amongst several renewable energy resources, solar energy has several advantages including its reliability, emission-free, eco-friendly and many more. Silicon-based solar cells are still in high demand due to the abundance of raw material, their high stability, non-toxicity and the compatibility of their fabrication with standard microelectronics industries [1], [2], [3]. To date, several attempts have been made to tackle the existing major challenges in silicon-based solar cells - to reduce the cost per watt by reducing the amount of material, increasing the efficiency and minimising the fabrication costs.

Amongst several solar cells available today, only the multijunction tandem solar cell delivers the potential to surpass the Shockley-Queisser limit, which is achieved by bandgap engineering [4], [5]. Along with quantum dots, silicon nanowires show potential to tailor the bandgap of crystalline silicon (C-Si) by controlling its dimensions at the nanoscale [2]. Currently, silicon nanowires (SiNWs) solar cells show efficiencies of approximately 12% by incorporating radial junction architectures using amorphous and crystalline silicon [6] and with surface passivation and texturing, the efficiency of SiNWs solar cells is further increased to 17% [7]; however, there is plenty of room to improve their efficiency. This can be achieved by several strategies including the heterojunction discussed in this paper. The use of SiNWs for solar cells shows several advantages including, enhanced absorption by trapping and scattering light, reduced reflection <5% compared to 40% in planar Si devices, collection of photo-generated carriers in different directions, efficient separation of charges due to large surface area, decoupling light absorption and charge transfer as light can be absorbed axially and carriers travel axially and radially to electrodes and these are, all achieved using less silicon compared to planar C-Si solar cells [2], [8], [9], [10], [11], [12], [13]. This research focuses on solar cells in which the junction is established by a crystalline wafer and crystalline nanowire (we term this as a wafer-wire junction). Several approaches have been reported to realise SiNW solar cells that utilise a crystalline nanowire core, which is covered with hydrogenated amorphous silicon to establish the junction [14], [15], [16], [17], [18]. This work eliminates the amorphous layers used in silicon nanowire solar cells. The use of amorphous silicon (a-Si) reduces both the stability and the efficiency of solar cells. Solar cells made using amorphous silicon suffer because of its low mobility and conductivity, high recombination rate and light-induced degradation due to the presence of defects in the material [19], [20]. Amorphous silicon heterostructures are still in use to increase the efficiency of solar cells due to the wider bandgap (~1.8 eV for a-Si) as compared with C-Si (1.12eV). This enhances the efficiency and the absorption of high energy photons. Photogenerated carrier separation and collection is also made more efficient due to the built-in field in the intrinsic a-Si layer deposited over C-Si, thus preventing photogenerated carriers from flowing to the undesirable side of the junction and thereby reducing recombination.

II. FABRICATION, Methods and CHARACTERISATION

Boron doped crystalline silicon wafers (1-10 ohm-cm, 200μm thick) single side polished, purchased from Pi-KEM-UK, are used for the fabrication of the solar cells. Silicon wafers were cleaned using an Radio Corporation of America (RCA) process and the native oxide was removed by dipping Si-wafers in a buffered hydrofluoric (HF) solution for 10 seconds and then rinsed thoroughly with deionised water to remove the residual HF. Aluminium (Al) bottom electrode was evaporated at 0.5nm/s at 1e-6 mBar base pressure to obtain a 200nm thick layer on the unpolished side of the silicon and annealed in a furnace at 500 ºC for 30 min in nitrogen ambience to form an ohmic contact. Then, silicon wafers and glass substrates (Corning-2875) were loaded in the thermal evaporator to

deposit 5nm mass thickness of Ga, In, Sn, Bi layers at 0.1nm/s at 1e-6 mBar base pressure. Then the wafer and glass with metal catalysts were loaded into the PECVD chamber for the growth of silicon nanowires. Hydrogen radical pre-treatment (Table I) is performed by hydrogen plasma to remove the superficial oxide layer over the metal and to control the density of nanoparticles. Following this, phosphine (PH_3) and silane (SiH_4) gases were introduced to grow n-type SiNWs (the growth conditions are listed in Table I).

TABLE I
PECVD PARAMETERS FOR ATOMIC HYDROGEN PLASMA TREATMENT AND GROWTH OF SINWS.

Deposition Parameters	H_2 radical pre-treatment	SiNWs growth process
H_2 Gas flow (SCCM)	100	100
SiH_4 Gas flow (SCCM)	-	20
PH_3 Gas Flow (SCCM)	-	2
RF power (W)	25	25
Temperature (ºC)	300	300
Pressure (mTorr)	200	200
Time (min)	5	10

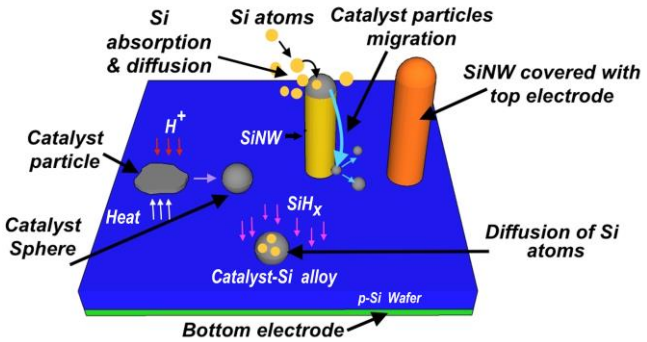

Fig. 1. One perspective image for understanding complete process Involved in the fabrication of solar cells. Detailed representation of catalyst nanoparticle formation, dissociation of SiH_x radicals, nucleation of catalyst seed, diffusion and precipitation of Si through the catalyst.

Samples are cooled down to room temperature in the PECVD chamber and immediately loaded in the thermal evaporator and the top contact is formed by evaporating silver through a shadow mask at 0.5nm/s at 1e-6 mBar base pressure to obtain a 500nm thick layer. Finally, fabricated solar cells are annealed rapidly at approximately 1000 °C for less than 3 seconds using a tungsten filament heater in a vacuum evaporator at 7e-7mBar base pressure. Fig. 1 describes the VLS process involved in the growth of the silicon nanowires. For Energy dispersive X-ray spectroscopy (EDX), X-ray diffraction (XRD) and Raman analysis (RENISHAW Micro-Raman system), SiNWs grown on the glass substrates are used.

III. RESULTS AND DISCUSSION

A. *SiNWs Growth and morphology*

Amongst the various metal catalysts used for the growth of SiNWs, this study focuses on Ga, In, Sn, Bi due to their relatively low eutectic temperature with silicon (below 300 ºC) as shown in the phase diagram (Fig. 2) and accompanying table (Table II). The melting point of all chosen catalysts coincides with the eutectic temperature and exhibits a steep liquefied line where the catalyst liquid alloy can be supersaturated with silicon at a range of temperatures from the eutectic temperature up to 500 ºC for gallium, 800 ºC for indium, 1000 ºC for bismuth and 600 ºC for tin.

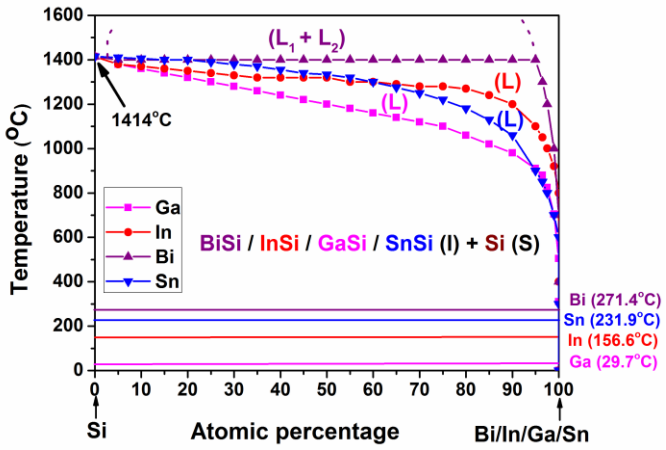

Fig. 2. Combinational plot with extrapolated data for better understanding of the binary phase diagrams of four metals with silicon reproduced from Olesinski and Mishra et al.

TABLE II
KEY PARAMETERS OF CATALYST AND THEIR VALUES WHICH ARE VITAL FOR UNDERSTANDING THE VLS GROWTH PROCESS.

Metals	Eutectic temp with Si (ºC)	Surface energy (J m^{-2})	Si Concentration in metal at eutectic Temp (at%)
Tin (Sn)	232	0.54 - 0.57	$<10^{-6}$
Indium (In)	156.6	0.50 - 0.56	$< 10^{-4}$
Gallium (Ga)	29.8	0.69 - 0.71	$< 10^{-8}$
Bismuth (Bi)	271.4	0.35 - 0.37	$<10^{-5}$
Gold (Au)	363	0.91 - 1.22	19

Also, all four chosen catalysts have low surface tension and exhibit a low silicon solubility of < 1 at% (values are included in Table II). Gibbs clarified that the surface tension (energy required/work done to increase the surface area) and surface free energy (energy required/work done to create a new area) of solids are not the same. Nebol's instability criterion indicates that it would be difficult for the growth of Si nanowires using low surface tension metals as a catalyst to grow silicon nanowires. Considering the surface energy of the solid (Silicon nanowire) $\sigma_s = 1.24$ J m^{-2}, Schmit et al showed that stable VLS growth process is achievable beyond the threshold surface tension of the liquid (metal catalyst) $\sigma_l = 0.85$ J m^{-2}. Although, the chosen metal catalysts do not meet this criterion, several reports, including this work demonstrate the growth of the nanowires using the aforementioned catalysts. Later, Yu and Mishra et al [21], [22] demonstrated that wetting of the catalyst at the sidewalls of the silicon nanowire help in stabilising the catalyst at the tip of the nanowires, especially for low surface tension metals.

Fig. 3 (first and second row) shows the morphologies of the catalyst (before and after H_2 plasma treatment) and SiNWs (third row). It should be noted evaporated catalyst are discontinuous in the form of nano-islands arranged in an irregular pattern (Fig. 3 first row). The density of the nanowires

depends on the density of the catalyst after hydrogen treatment; the density is controlled by the H_2 plasma parameters. Interestingly, the density of the spherical catalyst nanostructures increases with decreasing melting point of the respective catalysts. Similarly, the density of silicon nanowires is higher for the lower melting point catalyst such as Ga and lower for the higher melting point catalysts such as Bi used in this work. Periodic arrangement of nanowires in not important for light trapping and can be addressed by controlling the distance between the nanowires, diameter and the length of nanowires [23]. Hence, this work focused on trying to obtain nanowires of approximately 1um length, 100nm diameter and 200nm as the distance between nanowires for light trapping as observed in Fig. 3. Coupling of different wavelengths is difficult if nanowires are of the same diameter, as the coupling of higher wavelengths in thin nanowires and shorter wavelengths in thick nanowires is inefficient. In contrast to this, nanowires with a range of diameters is favourable in attaining high coupling efficiency at different wavelengths.

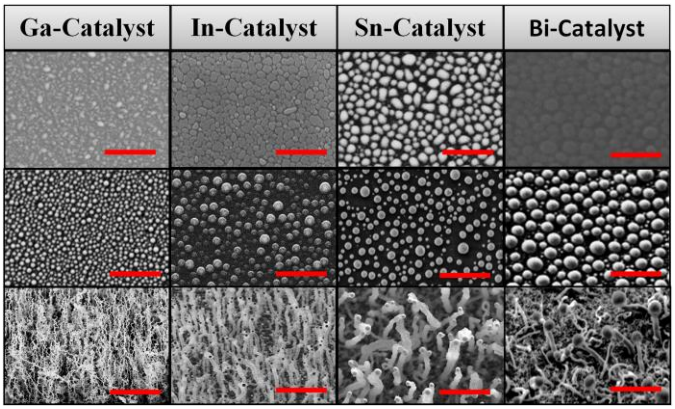

Fig. 3. Morphology of catalysts before (first row) and after (second row) H_2 plasma treatment. Morphology of SiNWs grown from mentioned catalysts (third row). The density (a number of nanowires per unit area) of nanowires depend on the density of catalyst droplets per unit area. Density of SiNWs is found to be decreasing with increasing eutectic temp of the catalyst with Si and/or melting point of the catalyst. Melting/Eutectic temperatures of Ga =29.8 °C, In = 156.6 °C, Sn - 232 °C, Bi = 271.4 °C. Scale bars in SEM images are 500nm.

TABLE III
DISTRIBUTION AND DIMENSIONS OF SINWS AT A SELECTED REGION IN SEM IMAGES FROM FIG 3, IT IS WORTH TO MENTION THAT THESE NUMBERS WILL VARRY ACROSS DIFFERENT REGIONS OF INTEREST.

Catalyst	Length (nm)	Diameter (nm)	Density (NWs/μm^{-2})
Bismuth (Bi)	240 ± 38	130 ± 31	15
Tin (Sn)	460 ± 22	180 ± 42	28
Indium (In)	360 ± 33	80 ± 24	58
Gallium (Ga)	880 ± 46	50 ± 7	140

B. Characterisation of SiNWs

The reflectivity of the Si wafer coated with metal catalyst nanoparticles on the polished surface increases for all wavelengths from 350nm to 1100nm and decreases from 200nm to 350nm (UV wavelengths). This behaviour is possible due to many factors that include size of the particle, polarization of light, gap between the particles, optical constants, interference of light (wave) and resonance exhibited by nanoparticles with diameters comparable to incident wavelengths. Reflection of the incident light strongly depends on the Refractive Index - RI (λ) and extinction co-efficient - k (λ) (note that RI and k values for a material are different for different wavelengths). Furthermore, the amount of interference depends on the RI (λ) of the overlaying layer (scattering nanostructures, anti-reflection thin films, encapsulation layer, etc.), in this work they are catalyst metal nanoparticles and the RI (λ) and the k (λ) of the underlying active layer (silicon). Therefore, reflectance of chosen metal nanoparticles is different at different wavelength of light. Furthermore, diameters of metal nanoparticles are comparable to the wavelengths corresponding to UV region where resonance scattering is higher leading to reduced reflection and/or increased absorption. Furthermore, the presence of the randomly arranged nanoparticles will cause interference with the incoming and scattered waves of light that results in the constructive or destructive interference. Hence, few wavelengths may have 0% reflectance compared to others that may have 50% or 100%, where the interference could either be completely destructive and/or partial destructive and/or fully constructive. Hence, reflectance will be different at range of wavelengths. Conversely, reflectivity is reduced for all the wavelengths after the growth of SiNWs on the Si wafer Fig. 4. The reflectivity of SiNWs on the Si Wafer is <15% in the entire range which indicates enhanced absorption of light caused by the silicon nanowires. This interesting light trapping and scattering property of SiNWs, when utilised for solar cells, obviates the need of an anti-reflection coating. The enhanced absorption and anti-reflective property is attributed to the refractive index gradient [24], resonant enhancement [25], increased optical path length [26] and diffuse reflectance.

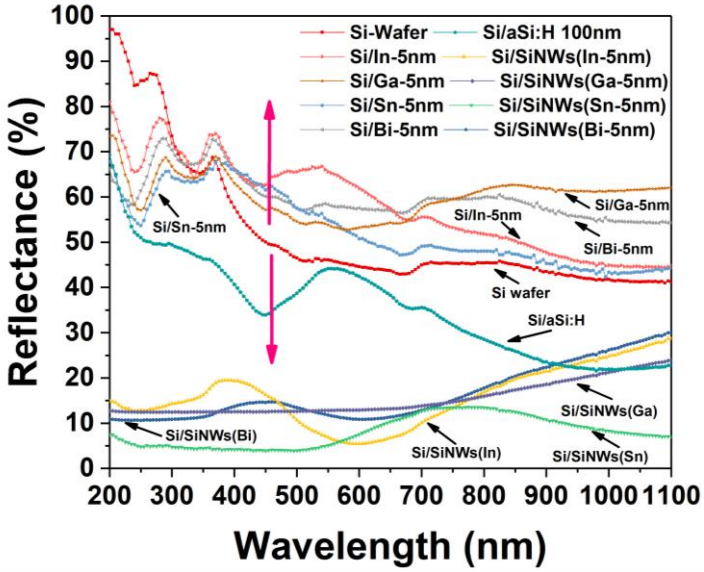

Fig. 4. Reflectance measurements of Si wafer coated with 5nm catalyst (In, Ga, Bi and Sn) showing an increase in reflectance compared with a reflectance of Si wafer and decrease in reflectance after the growth of SiNWs from In, Ga, Bi and Sn catalysts.

The chemical composition of as-grown SiNWs scratched from the glass substrate is sprinkled onto a Gallium-Arsenide (GaAs) wafer to eliminate the influence from the glass substrate that contains Si. The compositional peaks in the collected spectra

(Fig. 5) corresponding to Ga and As is from the substrate, the C peak is from the carbon tape used for supporting the substrate and O is either from a thin oxide layer at the surface of SiNWs and/or from the native oxide from GaAs substrate. Point analysis in performed for individual SiNW that shows a peak for Si, which confirms existence of Si in the bulk nanowire.

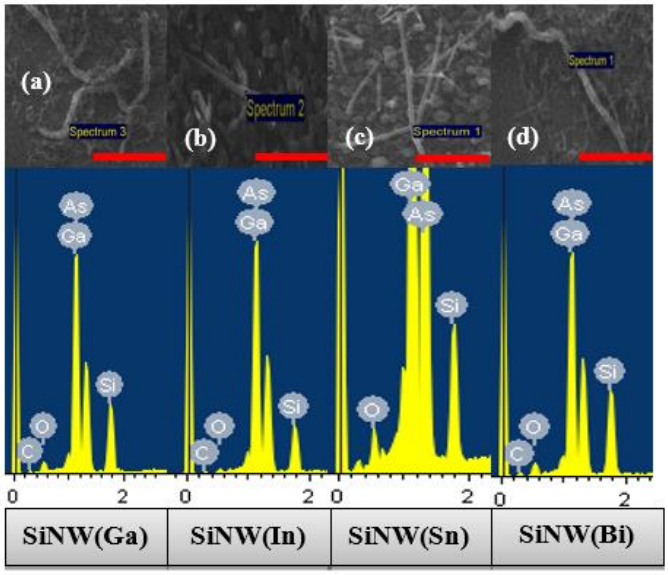

Fig. 5. Energy dispersive spectroscopy (point analysis) of SiNWs on GaAs substrate showing presence of Si in individual nanowire grown from Ga (a), In (b), Sn (c) and Bi (d) as labelled above. Collection time was 3 min for each sample and all scale bars are 500nm.

XRD analysis is also performed by gently sprinkling silicon nanowires (scratched from their glass substrates) onto a glass coated with a minute amount of vacuum grease. With the transfer technique used in this work, there is a possibility of breaking nanowires into smaller segments; however, there is no impact on the crystallinity as observed from the XRD data. The peak for metal catalyst observed in the spectra is due to their presence at the tip of SiNWs grown by the VLS process. Diffraction peaks depicted in the spectra corresponding to Si indicate that synthesised SiNWs are crystalline Fig. 6. Thicker nanowires grown from Sn show an intense diffraction peak corresponding to the Si (111) peak. For thin SiNWs grown from In this peak is reduced and further reduced in the much thinner SiNWs grown from Ga. SiNWs synthesised by the VLS process randomly grew in different crystal orientations for the catalysts used in this work. SiNWs grown from Bi had two additional diffraction peaks corresponding to Si (220) and (311) crystalline planes. SiNWs grown from Sn had four additional diffraction peaks corresponding to Si (220), (400), (422) and (333) crystal planes. SiNWs grown from Ga had an additional diffraction peak corresponding to the Si (220). SiNWs grown from In had two additional diffraction peaks corresponding to the Si (422) and (311). Presence of these peaks clearly indicate that SiNWs are crystalline.

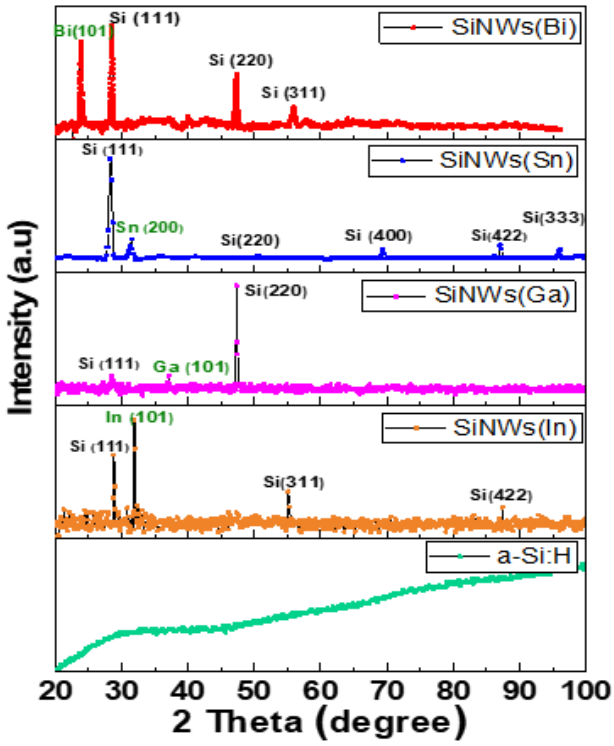

Fig. 6. Crystallinity analysis of SiNWs: XRD spectra of SiNWs grown from Sn, In, Bi and Ga catalysts including a-Si:H thin film.

The crystallinity of SiNWs is also analysed by Raman scattering measurements for SiNWs grown on a glass substrate (Fig. 7) along with XRD analysis discussed earlier. Raman measurements were conducted on SiNWs ensembles. Peaks at 516 cm-1, 512 cm^{-1}, 513 cm^{-1}, 502 cm^{-1} for SiNWs grown from Bi, Sn, In and Ga respectively indicate that SiNWs are crystalline, but, the peak positions are lower than the first order crystalline Si-Si transverse optic (1TO) excitation at about 520 cm^{-1}. This shift is thought to be related to local heating of nanowires induced by the laser during measurement [27] or mechanical strain in the nanowires. There is also a broad peak located at 298±2 cm^{-1} for SiNWs grown from all four catalysts corresponding to the Second-Order scattering observed in C-Si. Raman spectra depict absence of amorphous silicon for NWs grown from Sn and Bi. These NWs are shorter possibly due to the slow growth process which leads to better arrangement of atoms leading to higher order of crystalline growth [28] with reduced defects. SiNWs grown from Bi and Sn are mostly crystalline (darker contrast) with a negligible thickness of a-Si:H shell as seen in TEM images (Fig. 8 e &g). The shoulder in the peak representing a-Si:H from the Raman spectra obtained for SiNWs grown from In and Ga confirms the presence of a-Si:H shell. This can also be seen in the TEM images Fig. 8 d & i.

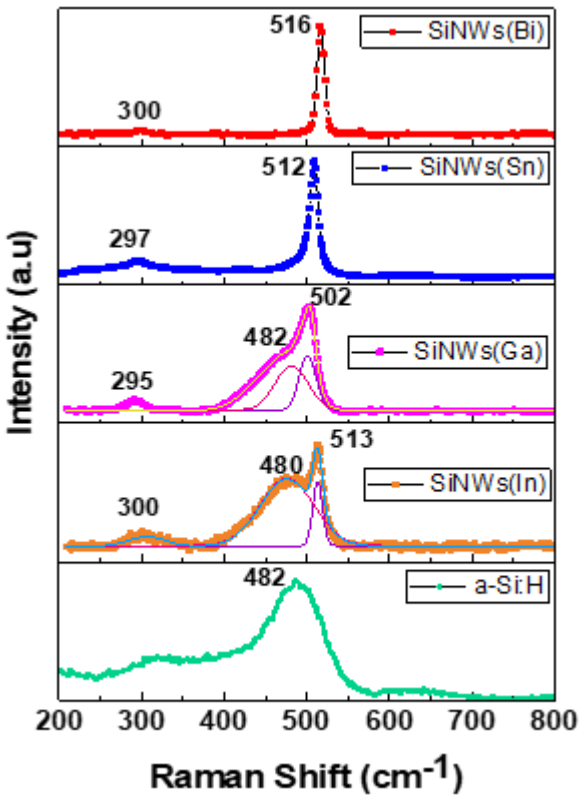

Fig. 7. Raman spectra of SiNWs grown from Sn, In, Bi and Ga catalysts showing first-order and second-order Raman scattering of silicon. Raman spectra was collected at an excitation wavelength of 633nm at 2.5mW laser power.

TEM investigation was performed to understand the individual nanowires to obtain better insight about their morphology. Kinks in the nanowires are possible due to the molten catalyst that is not held vertical to the nanowire during the growth process. This leads to a change in the growth direction every time the catalyst tip is displaced from the previous position (Fig. 8a). Tapering of nanowires is often observed in the SiNWs employed in the VLS growth process, with many reports suggesting that even sidewall parasitic deposition (Fig. 8d) could cause tapering [11], [29]. It is also possible that the volatile catalyst, at the tip of growing nanowire, being etched away during the growth, leading to a reduced precipitation of Si atoms at the region between the catalyst and the SiNW. In this work such phenomenon is observed for SiNWs grown from a highly volatile Bi catalyst (Fig. 8b). Interestingly, few SiNWs of diameters <10 nm are grown as branches to the parent vertical SiNW (diameter ≈ 60 nm). Such branched SiNWs (Fig. 8c) are observed only for Ga catalysed SiNWs. This may be attributed to the local supersaturation of the catalyst drops that wetted the nanowires, as the liquid catalyst flows along vertical down to the NW [9], [11]. This can be thought of as molten wax that flows along the vertical down to a burning candle. Additionally, Sn catalyst has shown simultaneous precipitation of twin nanowires from a single metal seed (Fig. 8h). Nanowires grown from In and Ga have crystalline Si core covered with thick a-Si:H shell (Fig. 8d&i). In a PECVD process due to availability of silane plasma, parasitic deposition of a-Si:H covering the nanowires is possible. Parasitic deposition of a-Si:H helps in passivation of SiNWs; which is an advantage of PECVD grown SiNWs. Conversely, SiNWs grown from Sn and Bi (Fig. 8e,f, g, j) do not have a thick a-Si:H shell; most region of the crystalline SiNWs is in darker contrast. Which is also reflected by XRD and Raman spectra showing SiNWs grown from Sn and Bi are mostly crystalline. In few NWs, certain regions within the nanowires, there are nanocrystallites with a grain size <20nm (Fig. 8j). Most of the nanowires have a crystalline core and/or region within the nanowire are crystalline.

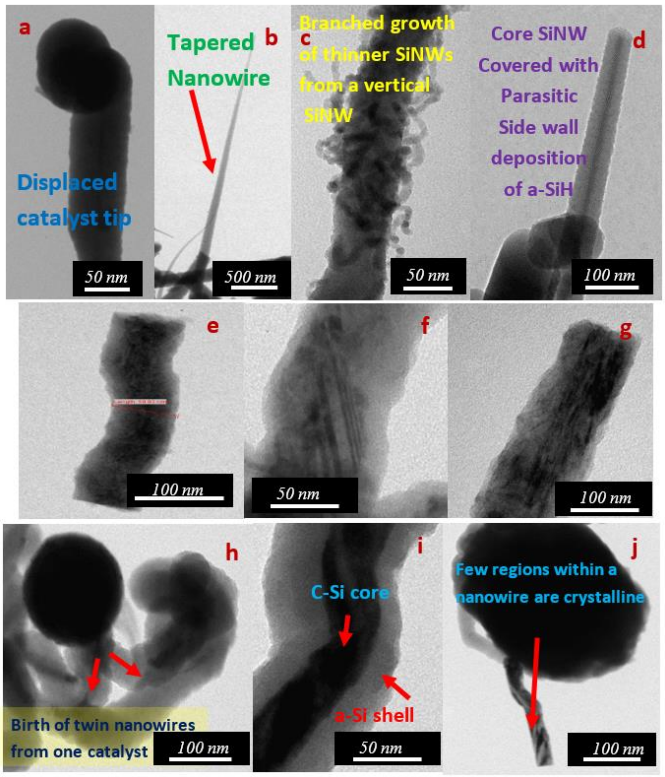

Fig. 8. Morphology of individual nanowires with several interesting hidden truths unfurled using TEM characterisation that provides better insight about SiNWs grown by plasma assisted VLS growth process. Growth of core crystalline SiNW covered with a-Si:H shell (d, i) that may lead to tapered SiNWs (d). Tapering of SiNWs grown from Bi is also observed when the catalyst size is reduced as it is removed by volatile Bi atoms (b). Few SiNWs grown from Sn has shown twin growth from one catalyst nanoparticle (h). Nanowires grown from Bi and Sn are mostly crystalline with negligible a-Si:H shell with most region of the NW is in darker contrast (e, g). Also, within these nanowires few regions are crystalline and remaining maybe amorphous (f, j).

C. Characterisation of SiNW solar cells

Solar cells fabricated in this work is based on P-N junction with top illumination as shown in Fig. 9. Phosphorus atoms from PH_3 gas are used to intentionally dope the SiNWs (n-type) grown from the different catalysts; however, catalyst also contributes towards doping the nanowires which we have published recently [30] and affected by the kinetic and thermodynamic factors associated with the size of nanomaterials [12]. Nanowires grown from In and Ga might have undergone unintentional counter doping from the catalyst as compared to SiNWs grown from Sn which has neutral/shallow energy levels in the forbidden gap of Si. The fabricated solar cell was edge isolated by dicing thin strips from all four edges after the evaporation of the top electrode.

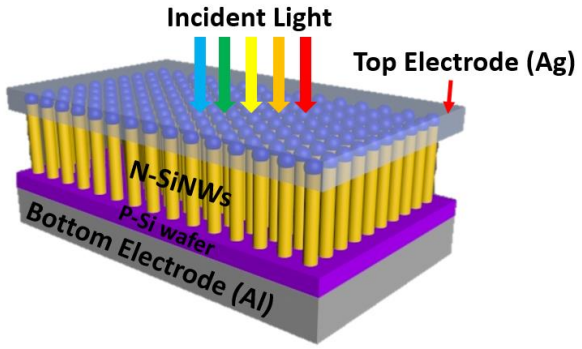

Fig. 9. Solar cell device structure designed for illumination of light from the top for illustrative purposes to provide more information about the structure.

The current-voltage (I-V) curves of solar cells, fabricated by SiNWs grown from different chosen catalysts, are shown in Fig. 10a. Image of Wafer-Wire junction solar cells on a 2cm x 2cm (Total substrate area = 4cm^2) p-Si substrate is shown in Fig. 10b with Ag top electrodes (with a contact area of 7.85e-3 cm^2 that is used for the electrical measurements). IV characteristics were measured by probing individual circular top Ag electrodes as shown in the Fig. 10c. In this scenario, as we don't know the exact contribution of the charge to electrical behaviour, it will be difficult to determine the current density and to find efficiency. This is because the dots are not connected and neither the current generated at one of the corners is reaching electrode that is being probed at another corner. Moreover, efficiency is not the scope of this study but understanding the contribution from the catalysts to the grown SiNWs that are used for the fabrication of solar cells.

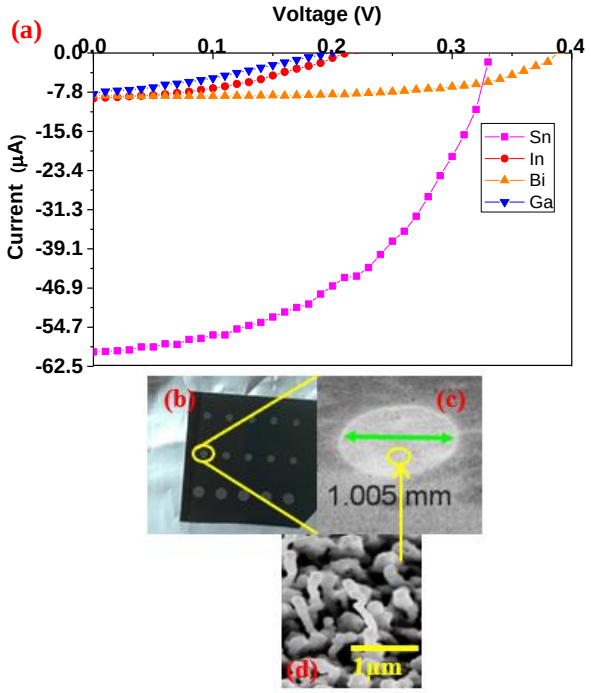

Fig. 10. Current –Voltage characteristics of the wafer-wire junction (p-Si wafer-n-Si nanowire) solar cells for nanowires grown from Sn, In, Ga and Bi catalyst (a). Optical and SEM images of solar cells showing top contacts (b-c) and SEM image of SiNW covered with top silver metal contact (d).

TABLE IV
MEASURED PARAMETERS OF WAFER-WIRE JUNCTION SOLAR CELLS WITH SINWS GROWN FROM DIFFERENT CATALYSTS TESTED UNDER 10E-3 W/CM^2 LIGHT SOURCE (AM 1.5G SPECTRUM) FOR TOP CIRCULAR AG ELECTRODE AREA = 7.85E-3 CM^2.

Metal catalyst	V_{oc} (V)	Isc (μA)	Power (P) = V_{oc} x I_{sc} (μW)	Normalised Power (N) = (P/19.73) x100
Tin (Sn)	0.33	59.8	19.73	100
Bismuth (Bi)	0.39	9.09	3.54	17.94
Indium (In)	0.21	8.08	1.69	8.56
Gallium (Ga)	0.19	8.58	1.63	8.26

Therefore, Normalised Power (N), which is a product of open circuit voltage (V_{oc}) and short-circuit current I_{sc}, is used to understand the choice of a suitable catalyst. A solar cell with SiNWs grown from a Sn catalyst is ideal with higher value of N (Table IV). Other three catalysts (Bi, Ga, In) that contribute towards nucleation, growth and doping of the SiNWs has lower value of N (<20) indicating that doping achieved by the use of PH_3 gas is altered and adversely affected due to potential catalysts metals that act as dopants in SiNWs. Please note that this mode-of-operandi is used for relative comparison among different solar cells fabricated using different catalysts. Solar cells fabricated from Bi catalysed SiNWs showed a lower value of short circuit current due to the reduced density of nanowires and dimensions (Fig. 3, Table III) as compared to the other devices and had an open circuit voltage of 0.39V. Increased Voc can be attributed to higher concentration of dopants leading to enhanced effective ionisation/activation rate in the SiNWs [31]. Solar cells fabricated from SiNWs made using the Ga and In catalysts have almost similar IV characteristics with low I_{sc} and V_{oc} compared to other two devices. A few publications [9], [32], report on wetting of SiNWs by these catalysts on the sidewalls of the nanowires, which is a possible recombination site for photo-generated charge carriers. This increases the dark saturation current that in turn decreases the open circuit potential. SiNWs grown from gallium are longer (≈1μm length) as compared, that exhibits a low V_{oc} due to the increase in the dark current as surface recombination is higher for longer nanowires. Nanowires grown from Ga also pose overshadowing effects due to the several bends and kinks causing a non-uniform coverage of the top contact and hence reduced Isc and also possibility of shunt paths will limit photo-current. Although silicon nanowires show good absorption, crystallinity and morphology, it is still problematical as to whether a high solar cell efficiency will be attained unless other key ingredients are thoroughly examined. The effect of wetting of the catalyst on the sidewall of SiNWs would enhance the recombination rate and increase the dark saturation current [33]. If growth conditions are not optimised for good morphology to provide kink free, reduced defects and reduced stacking faults in nanowires this would increase the series resistance and that can decrease the short circuit current. Removal of the catalyst tip is also vital for improving the efficiency of the solar cell [17].

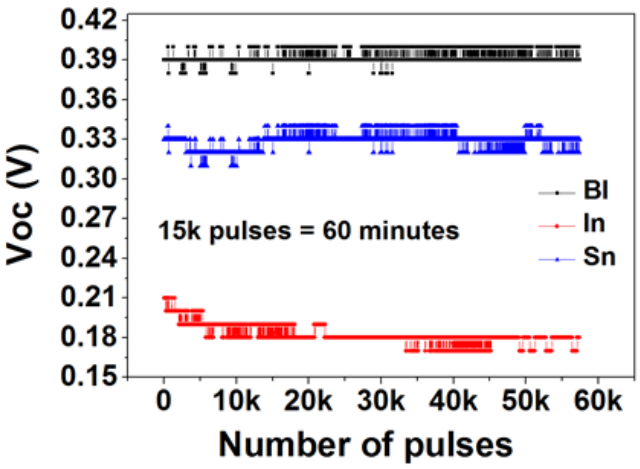

Fig. 11. Open circuit voltage of solar cell comprised of SiNWs grown from Bi, In, and Sn catalysts. V_{oc} was monitored for four hours approximately.

Solar cells discussed here do not have intentionally deposited amorphous silicon; both substrate and nanowire are crystalline where carrier lifetime is enhanced and thus contributing to the reduced recombination and enhanced charge carrier collection. Stability analysis was performed by measuring open circuit voltage with time (Fig. 11). Solar cells with SiNWs grown from Sn, Bi and In showed a negligible change of ±0.05V of Voc monitored for four hours. Due to large surface to volume ratio of SiNWs, heat generated in these kinds of solar cells is easily dissipated, while planar solar cells struggle to dissipate heat quickly.

IV. Conclusion

Nanowire-based solar cells can be grown from metal catalysts that have the same eutectic point as their melting point providing a range of temperatures for supersaturation from their eutectic temperature whilst still allowing the possibility of growing crystalline nanowires at low temperatures and eliminating the use of amorphous layers that deteriorate the performance of a solar cell with time. This report starts by describing the excellent properties of SiNWs that include light trapping by reduced reflection (enhanced absorption) that can be exploited to achieve higher efficiency in solar cells. A few potential challenges in the growth of silicon nanowires are discussed while suggesting how to address these issues. The range of low melting point metals is discussed for the growth of SiNWs that does not require higher temperatures and their important properties vital for solar cell research are discussed in brief. Enhanced absorption due to light trapping in SiNWs and efficient charge collection is demonstrated for improved performance in solar cells. We observe higher value of N for solar cells based on SiNWs grown from Sn. The reason for this is discussed by comparing results from several characterisation techniques. A lower value of N for the solar cells with SiNWs grown from Bi, In and Ga is due to unintentional doping performed by the catalyst along with the intentional doping n-type doping from PH_3. In general, performance of solar cells fabricated form SiNWs could be improved by obtaining better morphology of nanowires with adequate diameter and length whilst minimising the kinks and bends observed in such nanowires. Conformal coating of the top electrode on the nanowires is also important to minimise shunt paths. The etching of the catalyst at the tip and sidewalls of the nanowires has also played a vital role in increasing V_{oc} and I_{sc} as this reduces recombination of photo-generated carriers. We believe that a better efficiency could be observed in solar cells by engineering nanowires to communicate with light in a better way. To the best of our knowledge, we are amongst only three research groups demonstrating the growth of silicon nanowires from Bi catalyst. SiNWs grown from Bi are self-doped (n-type) and hence use of toxic gases such as PH_3 can be avoided and further simplifying the optimisation process of fabrication of electronic devices (including photovoltaic solar cells). This report compares various catalysts for the growth of nanowires discussing their properties, and such wires can be utilised in several other applications not only limited to photovoltaic research.

Author Contributions

Krishna Nama Manjunatha and Shashi Paul designed the experiment, analysed the data and co-wrote the article. Iulia Salaoru has only collected the XRD data for SiNWs grown from Sn presented in Fig 6. W.I Milne made a number of important suggestions and edited the manuscript. Most of the experimental work was carried out at EMTERC, De Montfort University.

Acknowledgment

Shashi Paul would like to thank the EPSRC (#EP/P020518/1) for their financial support.

References

[1] K. -. Peng, X. Wang, L. Li, Y. Hu and S. -. Lee, "Silicon nanowires for advanced energy conversion and storage," *Nano today*, vol 8, no 1, pp. 75-97, 2013.

[2] J. K. Mann, R. Kurstjens, G. Pourtois, M. Gilbert, F. Dross and J. Poortmans, "Opportunities in nanometer sized si wires for PV applications," *Progress in materials science*, vol 58, no 8, pp. 1361-1387, 2013.

[3] T. Song, S. Lee and B. Sun, "Silicon nanowires for photovoltaic applications: The progress and challenge," *Nano energy*, vol 1, no 5, pp. 654-673, 2012.

[4] Y. Hou, E. Aydin, M. De Bastiani, C. Xiao, F. H. Isikgor, D. Xue, B. Chen, H. Chen, B. Bahrami and A. H. Chowdhury, "Efficient tandem solar cells with solution-processed perovskite on textured crystalline silicon," *Science*, vol 367, no 6482, pp. 1135-1140, 2020.

[5] M. I. Hossain, W. Qarony, S. Ma, L. Zeng, D. Knipp and Y. H. Tsang, "Perovskite/silicon tandem solar cells: From detailed balance limit calculations to photon management," *Nano-micro letters*, vol 11, no 1, pp. 58, 2019.

[6] A. S. Togonal, M. Foldyna, W. Chen, J. X. Wang, V. Neplokh, M. Tchernycheva, J. Nassar and P. Roca i Cabarrocas, "Coreâ€“shell heterojunction solar cells based on disordered silicon nanowire arrays," *The journal of physical chemistry C*, vol 120, no 5, pp. 2962-2972, 2016.

[7] X. X. Lin, X. Hua, Z. G. Huang and W. Z. Shen, "Realization of high performance silicon nanowire based solar cells with large size," *Nanotechnology*, vol 24, no 23, pp. 235402, 2013.

[8] K. Peng, Y. Xu, Y. Wu, Y. Yan, S. Lee and J. Zhu, "Aligned Single-Crystalline si nanowire arrays for photovoltaic applications," *Small*, vol 1, no 11, pp. 1062-1067, 2005.

[9] N. Gabrielyan, K. Saranti, K. N. Manjunatha and S. Paul, "Growth of low temperature silicon nano-structures for electronic and electrical energy generation applications," *Nanoscale research letters*, vol 8, no 1, pp. 1-7, 2013.

[10] Linwei Yu, "Radial junction amorphous silicon solar cells on PECVD-grown silicon nanowires," *Nanotechnology*, vol 23, no 19, pp. 194011, 2012.

[11] S. Misra, L. Yu, W. Chen, M. Foldyna and P. Roca I Cabarrocas, "A review on plasma-assisted VLS synthesis of silicon nanowires and radial junction solar cells," *Journal of physics D: Applied physics*, vol 47, no 39, 2014.

[12] P. Xie, Y. Hu, Y. Fang, J. Huang and C. M. Lieber, "Diameter-dependent dopant location in silicon and germanium nanowires," *Proceedings of the national academy of sciences*, vol 106, no 36, pp. 15254-15258, 2009.

[13] K. N. Manjunatha and S. Paul, "Carrier selective metal-oxides for self-doped silicon nanowire solar cells," *Applied surface science*, vol 492, pp. 856-861, 2019.

[14] M.M. Adachi and K.S. Karim, , "Fabrication of PECVD grown n-i-p silicon nanowire solar cells," In *Conference record of the IEEE photovoltaic specialists conference*, 2010, pp. 3302-3305.

[15] M.M. Adachi, M.P. Anantram and K.S. Karim, *Core-shell silicon nanowire solar cells*, 2013Available from: http://dx.doi.org/10.1038/srep01546.

[16] E. S. Ashour, M. Y. B. Sulaiman, M. H. Ruslan and K. Sopian, "A-si:H/SiNW shell/core for SiNW solar cell applications," *Nanoscale research letters*, vol 8, no 1, pp. 466, 2013.

[17] B. O'Donnell, L. Yu, M. Foldyna and P. Roca I Cabarrocas, "Silicon nanowire solar cells grown by PECVD," *Journal of non-crystalline solids*, vol 358, no 17, pp. 2299-2302, 2012.

[18] J. Cho, B. O'Donnell, L. Yu, K. -. Kim, I. Ngo and P. R. I. Cabarrocas, "Sn-catalyzed silicon nanowire solar cells with 4.9% efficiency grown on glass," *Progress in photovoltaics: Research and applications*, vol 21, no 1, pp. 77-81, 2013.

[19] F. Meillaud, M. Boccard, G. Bugnon, M. Despeisse, S. Hänni, F. -. Haug, J. Persoz, J. -. Schüttauf, M. Stuckelberger and C. Ballif, "Recent advances and remaining challenges in thin-film silicon photovoltaic technology," *Materials today*, vol 18, no 7, pp. 378-384, 2015.

[20] M. Fehr, A. Schnegg, B. Rech, O. Astakhov, F. Finger, R. Bittl, C. Teutloff and K. Lips, "Metastable defect formation at microvoids identified as a source of light-induced degradation in a - si: H," *Physical review letters*, vol 112, no 6, 2014.

[21] S. Misra, L. Yu, W. Chen and P. Roca I Cabarrocas, "Wetting layer: The key player in plasma-assisted silicon nanowire growth mediated by tin," *Journal of physical chemistry C*, vol 117, no 34, pp. 17786-17790, 2013.

[22] L. Yu, B. O'Donnell, P. -. Alet, S. Conesa-Boj, F. Peiró, J. Arbiol and P. R. I. Cabarrocas, "Plasma-enhanced low temperature growth of silicon nanowires and hierarchical structures by using tin and indium catalysts," *Nanotechnology*, vol 20, no 22, 2009.

[23] M. Foldyna, L. Yu, S. Misra and P. Roca I Cabarrocas, , "Light trapping enhancement in ordered and disordered silicon nanowire based solar cells," In *Proceedings of SPIE - the international society for optical engineering*, 2013, .

[24] B. -. Huang, Y. -. Yang, T. -. Lin and W. -. Yang, "A simple and low-cost technique for silicon nanowire arrays based solar cells," *Solar energy materials and solar cells*, vol 98, pp. 357-362, 2012.

[25] G. Grzela, D. Hourlier and J. Gómez Rivas, "Polarization-dependent light extinction in ensembles of polydisperse vertical semiconductor nanowires: A mie scattering effective medium," *Physical review B - condensed matter and materials physics*, vol 86, no 4, 2012.

[26] K. N. Manjunatha and S. Paul, "In-situ catalyst mediated growth and self-doped silicon nanowires for use in nanowire solar cells," *Vacuum*, vol 139, pp. 178-184, 2017.

[27] P. -. Alet, L. Yu, G. Patriarche, S. Palacin and P. Roca i Cabarrocas, "In situ generation of indium catalysts to grow crystalline silicon nanowires at low temperature on ITO," *Journal of materials chemistry*, vol 18, no 43, pp. 5187-5189, 2008.

[28] K. K. Ostrikov, I. Levchenko, U. Cvelbar, M. Sunkara and M. Mozetic, "From nucleation to nanowires: A single-step process in reactive plasmas," *Nanoscale*, vol 2, no 10, pp. 2012-2027, 2010.

[29] L. Yu, F. Fortuna, B. O'Donnell, T. Jeon, M. Foldyna, G. Picardi and P. Roca I Cabarrocas, "Bismuth-catalyzed and doped silicon nanowires for one-pump-down fabrication of radial junction solar cells," *Nano letters,* vol 12, no 8, pp. 4153-4158, 2012.

[30] K. Nama Manjunatha and S. Paul, "In-situ catalyst mediated growth and self-doped silicon nanowires for use in nanowire solar cells," *Vacuum,* vol 139, pp. 178-184, 2017.

[31] L. Yu, F. Fortuna, B. Oâ€™Donnell, T. Jeon, M. Foldyna, G. Picardi and P. Roca i Cabarrocas, "Bismuth-catalyzed and doped silicon nanowires for one-pump-down fabrication of radial junction solar cells," *Nano letters,* vol 12, no 8, pp. 4153-4158, 2012.

[32] A. K. Muhammad, Y. Ishikawa, I. Kita, A. Tani, H. Yano, T. Fuyuki and M. Konagai, "Investigation of crystallinity and planar defects in the si nanowires grown by vapor-liquid-solid mode using indium catalyst for solar cell applications," *Japanese journal of applied physics,* vol 55, no 1, 2016.

[33] C. Yung Kuo, C. Gau and B. Tong Dai, "Photovoltaic characteristics of silicon nanowire arrays synthesized by vaporliquidsolid process," *Solar energy materials and solar cells,* vol 95, no 1, pp. 154-157, 2011.